for D atoms in pure glycerol is calculated to be 5 ns. D-atom desorption competes nearly equally with D-atom reaction; these atoms desorb on average over a depth of $(Dt_{1/2})^{1/2} \approx 50$ Å, or ~10 glycerol layers, using a diffusion coefficient $D \approx 4 \times 10^{-5}$ cm$^2$ s$^{-1}$ for D atoms in $D_2O$ (*23*, *24*). This reaction depth may even be shallower if the D atoms diffuse more slowly in pure glycerol because of its viscosity, 2800 cP, at 287 K (*13*). D atoms are therefore created by $e_s^-$ close to, but not necessarily within, the outermost region where Na atoms ionize (*15*).

Figure 4 summarizes the production of D, $D_2$, $D_2O$, and glycerol fragments initiated by surface Na-atom ionization, along with possible scenarios for their creation. Each species desorbs only after thermal equilibration. This observation is complementary to the nonthermal ejection of D and O atoms after bombardment of $D_2O$ ice by electrons carrying 5 to 50 eV of energy (*25*), which is substantially greater than the −0.8 eV ionization enthalpy of Na in bulk water (*26*, *27*). Analysis of the TOF signals (table S2) indicates that D, $D_2$, and $D_2O$ desorb in the flux ratio 1:1.3:3.2. We thus find that nearly half of the D atoms produced by electron-stimulated dissociation of O-D and C-D bonds escape into the vacuum before they abstract a second D atom from the solvent to produce $D_2$. This high desorption rate implies that near-surface reactions of even this energetic species must compete with its escape into the vacuum—a route that is not available deep within glycerol or other solvents, potentially including aqueous solutions. Because of the proximity of surface molecules to the gas phase, the observed competition between evaporation and reaction should be a universal feature of the interfacial chemistry of neutral energetic species created by interfacial electrons. Alkali-atom collisions provide a promising approach to prepare these electrons and the radicals they create, and to explore their reactions with both solvent and solute molecules at or near the surfaces of liquids.

### References and Notes


1. B. C. Garrett *et al.*, *Chem. Rev.* **105**, 355 (2005).
2. G. V. Buxton, C. L. Greenstock, W. P. Helman, A. B. Ross, W. Tsang, *J. Phys. Chem. Ref. Data* **17**, 513 (1988).
3. N. I. Hammer *et al.*, *Science* **306**, 675 (2004).
4. J. R. R. Verlet, A. E. Bragg, A. Kammrath, O. Cheshnovsky, D. M. Neumark, *Science* **307**, 93 (2005).
5. Á. Madarász, P. J. Rossky, L. Turi, *J. Chem. Phys.* **126**, 234707 (2007).
6. D. M. Sagar, C. D. Bain, J. R. R. Verlet, *J. Am. Chem. Soc.* **132**, 6917 (2010).
7. K. R. Siefermann *et al.*, *Nat. Chem.* **2**, 274 (2010).
8. B. Abel, U. Buck, A. L. Sobolewski, W. Domcke, *Phys. Chem. Chem. Phys.* **14**, 22 (2012).
9. A. H. Muenter, J. L. DeZwaan, G. M. Nathanson, *J. Phys. Chem. B* **110**, 4881 (2006).
10. J. Bonin, I. Lampre, P. Pernot, M. Mostafavi, *J. Phys. Chem. A* **112**, 1880 (2008).
11. R. N. Barnett, R. Giniger, O. Cheshnovsky, U. Landman, *J. Phys. Chem. A* **115**, 7378 (2011).
12. M. E. Saecker, G. M. Nathanson, *J. Chem. Phys.* **99**, 7056 (1993).
13. See supporting material on *Science* Online.
14. J. Zhang, D. J. Garton, T. K. Minton, *J. Chem. Phys.* **117**, 6239 (2002).
15. L. Cwiklik, U. Buck, W. Kulig, P. Kubisiak, P. Jungwirth, *J. Chem. Phys.* **128**, 154306 (2008).
16. Y. Ferro, A. Allouche, V. Kempter, *J. Chem. Phys.* **120**, 8683 (2004).
17. R. M. Forck *et al.*, *J. Chem. Phys.* **132**, 221102 (2010).
18. D. H. Paik, I.-R. Lee, D.-S. Yang, J. S. Baskin, A. H. Zewail, *Science* **306**, 672 (2004).
19. J. J. J. Myron, G. R. Freeman, *Can. J. Chem.* **43**, 381 (1965).
20. C. E. Burchill, K. M. Perron, *Can. J. Chem.* **49**, 2382 (1971).
21. J. Park, Z. F. Xu, M. C. Lin, *J. Chem. Phys.* **118**, 9990 (2003).
22. A. M. Lossack, E. Roduner, D. M. Bartels, *J. Phys. Chem. A* **102**, 7462 (1998).
23. E. Roduner, *Radiat. Phys. Chem.* **72**, 201 (2005).
24. V. A. Benderskii, A. G. Krivenko, *Russ. J. Electrochem.* **32**, 663 (1996).
25. T. M. Orlando, G. A. Kimmel, *Surf. Sci.* **390**, 79 (1997).
26. J. O. M. Bockris, A. K. N. Reddy, *Modern Electrochemistry I: Ionics* (Plenum, New York, ed. 2, 1998).
27. H. Shiraishi, G. R. Sunaryo, K. Ishigure, *J. Phys. Chem.* **98**, 5164 (1994).



**Acknowledgments:** This work was supported by NSF grant CHE-0943639 as part of the Center for Energetic Non-Equilibrium Chemistry at Interfaces. We thank L. Sankaran, G. Schatz, I. Benjamin, and a reviewer for invaluable advice. The data described in this work can be obtained from the corresponding authors upon request.


### Supporting Online Material

www.sciencemag.org/cgi/content/full/335/6072/1072/DC1
Materials and Methods
SOM Text
Figs. S1 and S2
Tables S1 and S2
References (*28*–*36*)


31 October 2011; accepted 25 January 2012
10.1126/science.1215956


# No Straight Path: Roaming in Both Ground- and Excited-State Photolytic Channels of $NO_3 \rightarrow NO + O_2$


**Michael P. Grubb,[1] Michelle L. Warter,[1] Hongyan Xiao,[2] Satoshi Maeda,[2,3] Keiji Morokuma,[2,4] Simon W. North[1]***



**Roaming mechanisms have recently been observed in several chemical reactions alongside trajectories that pass through a traditional transition state. Here, we demonstrate that the visible light–induced reaction $NO_3 \rightarrow NO + O_2$ proceeds exclusively by roaming. High-level ab initio calculations predict specific NO Λ doublet propensities (orientations of the unpaired electron with respect to the molecular rotation plane) for this mechanism, which we discern experimentally by ion imaging. The data provide direct evidence for roaming pathways in two different electronic states, corresponding to both previously documented photolysis channels that produce $NO + O_2$. More broadly, the results raise intriguing questions about the overall prevalence of this unusual reaction mechanism.**


Traditionally, chemical reaction mechanisms involving multiple bond breaking and formation steps are characterized by a transition state in the form of a well-defined saddle point on the potential energy surface. Recently, however, a second type of mechanism termed "roaming" has come to light, which bypasses this saddle point entirely (*1*–*3*). Instead, a frustrated bond cleavage leaves part of the molecule without sufficient energy to escape, and it orbits the remaining fragment until encountering a reactive site to form the products via intramolecular abstraction. This mechanism has received considerable attention in the past 8 years, having been first identified in formaldehyde dissociation as a minor channel (*4*, *5*) and then later in acetaldehyde as the dominant pathway to $CH_4 + CO$ products (albeit still a minor fraction of the overall quantum yield) (*6*, *7*). Evidence of roaming dynamics has since been observed in a handful of other systems, but in all cases has been observed alongside a traditional tight transition state channel (*2*, *8*).

Recently, we reported that roaming may be the dominant of the two observed pathways that produce molecular products in $NO_3$ photodissociation (*9*), a reaction of considerable atmospheric importance. Additionally, theoretical calculations implicated roaming on the excited-state potential surface; previous observations of roaming were restricted to the electronic ground state (*10*, *11*). Here, we report direct experimental and theoretical evidence confirming the role of excited-state roaming in $NO_3$ photodissociation. Thus, roaming is not only the dominant mechanism for forming the molecular products of $NO_3$ but the exclusive mechanism, with no evidence of a competing traditional transition state.


[1]Department of Chemistry, Texas A&M University, College Station, TX 77842, USA. [2]Fukui Institute for Fundamental Chemistry, Kyoto University, 34-4 Takano Nishihiraki-cho, Sakyo, Kyoto 606-8103, Japan. [3]The Hakubi Center, Kyoto University, Yoshida-Ushinomiya-cho, Sakyo-ku, Kyoto 606-8302, Japan. [4]Cherry L. Emerson Center for Scientific Computation and Department of Chemistry, Emory University, Atlanta, GA 30322, USA.

*To whom correspondence should be addressed. E-mail: swnorth@tamu.edu

The two dissociative pathways of $NO_3$ to yield NO and $O_2$ products were recently resolved via high-resolution ion imaging experiments (*9*, *12*). In those experiments, a molecular beam of dilute $NO_3$ (<1%) in helium was photolyzed by a 588-nm laser pulse. A single rovibronic quantum state of the NO photofragment was selectively ionized by a second laser, and the resulting NO cations were focused by electrostatic lenses onto a two-dimensional microchannel plate–phosphor ion detector. The radial displacement of each ion impact is a measure of the recoil velocity resulting from the photolysis. By simultaneously measuring the NO quantum state and velocity, the quantum state of the coincident $O_2$ fragment could be determined through the conservation of energy and linear momentum. State-selective correlated measurements are ideal for uncovering multiple reaction pathways and revealed two separate pathways for the $NO_3 \rightarrow NO + O_2$ reaction. Pathway 1 (Pwy 1), the dominant pathway, resulted in highly vibrationally excited $O_2$ fragments in coincidence with lower NO rotational quantum numbers (Fig. 1, inset). This pathway bears many similarities to the roaming pathway observed in formaldehyde dissociation. The excited $O_2$ vibrational distribution originates from the extended O-O bond distance at the roaming saddle point (ONO-O). Vibrationally excited $O_2$ products ($v > 6$) have also been observed in the intermolecular abstraction reaction $NO_2 + O \rightarrow NO + O_2$ (*13*), reinforcing the description of roaming as an intramolecular abstraction (*14*, *15*).

The nature of pathway 2 (Pwy 2), which results in fragments with large rotational angular momentum in both products and a colder $O_2$ vibrational distribution (Fig. 1, inset), has proven more elusive. Although it was speculated that the pathway originated from a traditional three-center transition state (*12*, *16*), which is present in all other systems where roaming has been identified, no transition state of relevant energy has yet been calculated by theory. Recent theoretical calculations mapping the potential energy surfaces of the first several electronic states of $NO_3$ have shown that the lowest-lying excited state, which is optically dark, is accessible through a series of conical intersections after photoexcitation to a higher-energy "bright" state (Fig. 1) (*10*). Maeda and co-workers proposed that roaming actually occurs on this first excited dark state and may later access the ground state at long ($O_2$N-O) bond distances through another conical intersection. The two experimentally observed pathways could therefore be explained by dissociation on two different electronic potential surfaces (*10*, *11*). Furthermore, the ONO-O saddle point on each potential surface (SP1 and SP2) has a different O-O bond length leading to different vibrational distributions in the $O_2$ product fragment, consistent with experimental observations. The critical role of the optically dark state in the photochemistry of $NO_3$ was unexpected and warranted further experimental exploration.

An experimental test of this two-state roaming theory requires that a signature of the dissociative electronic state be retained in the photofragments. Electronic symmetry must be conserved for chemical processes, and thus the electronic orbital symmetry in $NO_3$ should be maintained in the product fragments. The orbital symmetry of a diatomic molecule in a $^2\Pi$ electronic configuration such as the ground state of NO can be expressed by the $\Lambda$ doublet propensity. An A" $\Lambda$ doublet propensity indicates that the singly occupied p$\pi$-orbital lobe is pointed out of the fragment rotational plane, whereas an A' $\Lambda$ doublet propensity indicates that the lobe is oriented in the rotational plane. The photodissociation of water is a classic example of this electronic symmetry conservation. The absorption of a photon leads to an excited electronic state of water characterized by an unpaired electron in an out-of-plane p$\pi$-orbital lobe. This symmetry is conserved during dissociation, resulting

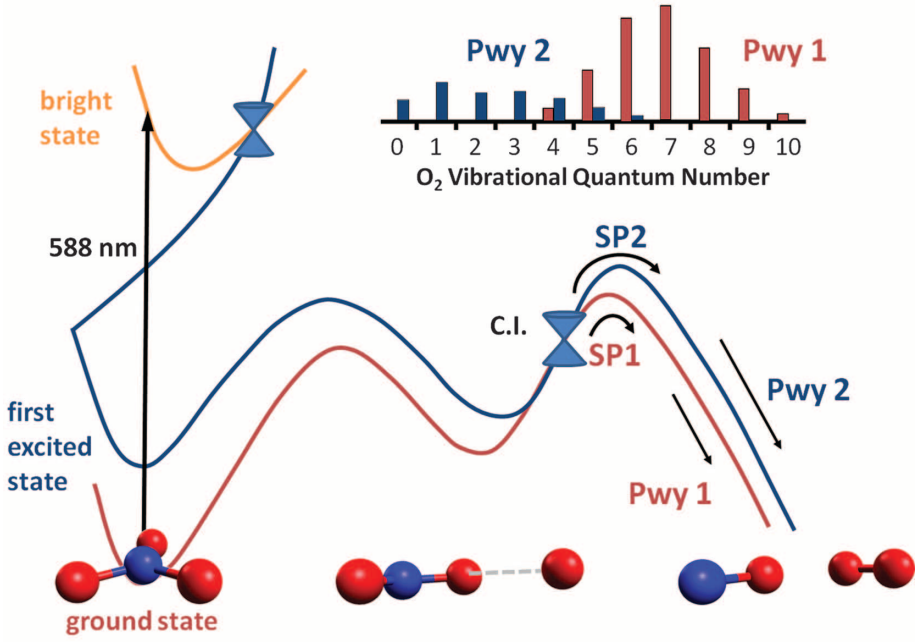


**Fig. 1.** Schematic diagram of the lowest-lying electronic state surfaces proposed to give rise to the two experimentally observed pathways (Pwy 1 and 2) via C.I. (conical intersection) resulting from $NO_3$ photolysis at 588 nm. The experimental vibrational distributions of the $O_2$ fragments produced from the two pathways are also provided, with the difference ascribed to different ONO-O bond lengths at the saddle points on the two surfaces (SP1 and SP2).

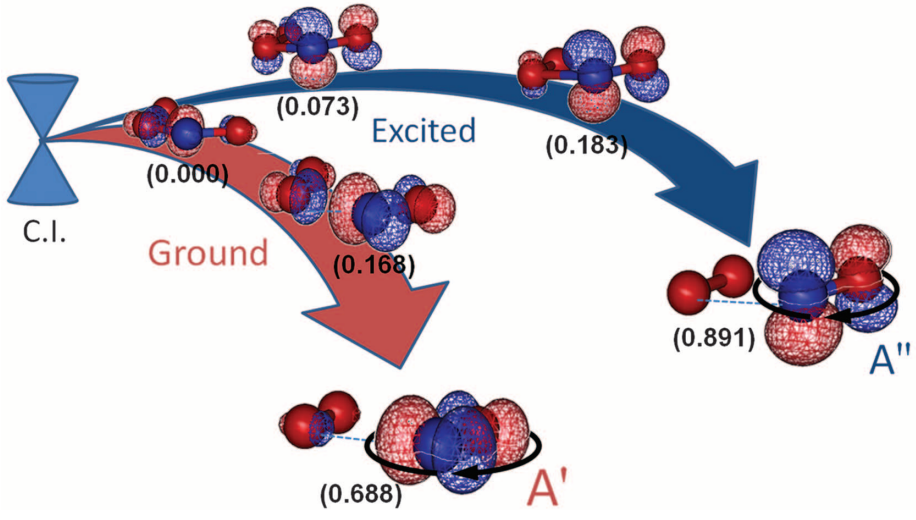


**Fig. 2.** Evolution of the key electronic orbital in the $NO_3$ exit channel derived from the CASSCF calculations (*18*) of some representative structures along the post-C.I. reaction pathways determined by our previous study (*10*). The occupancy of the orbital is shown at each step in parentheses. In-plane dissociation results in opposite NO $\Lambda$ doublet propensities for the two pathways.

in a strong preference for producing OH fragments in the upper A" Λ doublet state, from which stimulated emission has been proposed as a source for interstellar masers (*17*). The correlation between Λ doublet propensities and electronic origin provides a convenient means of distinguishing pathways on different electronic potential surfaces, provided the electronic states possess different electronic symmetries.

We performed ab initio calculations to determine the evolution of the electronic orbitals in the $NO_3$ exit channel, in order to predict the preferred Λ doublet state arising from each electronic state potential surface. These orbitals were obtained by CASSCF calculations (*18*) and calculated for some representative structures along the reaction pathways determined in our previous study (*10*). The results shown in Fig. 2 support in-plane dissociation on both surfaces (*19*) and conveniently predict opposite Λ doublet propensities for each pathway. The pπ-orbital lobe in the NO fragment containing the unpaired electron lies in the NO rotational plane (A' Λ doublet state) for trajectories evolving on the ground state of $NO_3$, whereas the lobe is perpendicular to the NO rotational plane (A" Λ doublet state) for trajectories evolving on the dark state of $NO_3$. Thus, experimental measurements of the NO Λ doublet propensities should show an A' preference for pathway 1 and an A" preference for pathway 2, if the two-state dissociation model is correct (*20*).

The unpaired pπ-orbital lobe in NO defines the spectroscopic transition dipole moment **μ** for the $A(^2\Sigma) \leftarrow X(^2\Pi)$ transition, which is the resonant step of the two-photon detection scheme previously used in the ion imaging experiments of (*9*, *12*). The Λ doublet propensity of the NO fragment can therefore be determined by comparing the relative intensities of the P, Q, and R branches of this transition (*21*). For a classical Q branch transition, **μ** is parallel to the rotational axis **j**. Therefore, a Q branch transition will primarily excite the A" Λ doublet state, where the unpaired pπ-orbital lobe and hence **μ** is pointing out of the rotational plane along **j**. For a P or R branch transition, **μ** is perpendicular to **j** and thus the A' Λ doublet state is preferred. In the case of our ion imaging experiments, the two dissociation pathways result in NO fragments with two different translational energy distributions (observed as different radii in the ion images). Relative Λ doublet propensities for the two pathways can therefore be determined by observing how the relative intensity of the two energy distributions changes when the NO is detected via Q and P (or R) branch transitions. Previous measurements of rotationally excited NO fragments focused on Q branch transitions, as the lines of this branch are more isolated in the excitation spectrum. Here, we present measurements of a particular NO rotational state probed via multiple rotational branches (*18*).

Figure 3 shows velocity map images of the NO ($^2\Pi_{3/2}$ $v = 0$, $N = 22$) photoproducts after resonance-enhanced multiphoton ionization, as well as the corresponding NO total translational energy distributions, probed via the $Q_{22}$ branch (right) and the $P_{22}$ branch (left). The lower–translational energy NO fragments originate from pathway 1 (because most of the available energy is in the vibration of the $O_2$ cofragment), whereas the higher–translational energy NO originates from pathway 2. The results are dramatic, showing highly suppressed pathway 2 signal in the $P_{22}$ branch ion image. This implies a strong preference in pathway 2 for producing NO in the A" Λ doublet state, in agreement with the theoretical prediction shown in Fig. 2. The magnitude of the difference in the relative intensities also suggests that NO derived from pathway 1 must possess the opposite Λ doublet propensity, in agreement with the ab initio calculations, although this result is not necessarily of dynamical origin because a 2:1 ratio favoring the A' state is statistically predicted if the dissociation is not constrained to the molecular plane (*22*).

The results of these measurements and the corresponding theory strongly support in-plane two-state roaming dynamics for $NO_3$ photodissociation, without competition from a traditional transition state mechanism. Additionally, the $NO_3$ system differs from previous documented roaming dissociations in that its roaming dynamics access multiple electronic potential surfaces. Near the product asymptotes the electronic potentials converge, and because roaming trajectories explore a large area of these asymptotic surfaces, it is not surprising that the trajectories may involve multiple electronic states. What effect does the slow, broadly sampling dynamics of roaming have on a system's ability to access additional potential energy surfaces? Do roaming dynamics lead to an even more complicated reaction than a simple intramolecular abstraction? The low vibrational states of the oxygen fragment associated with the dark state pathway could not be measured due to diminishing Franck-Condon factors in previous laser-induced fluorescence experiments. It is therefore unclear whether the excited state is accessed in the bimolecular $NO_2 + O$ abstraction reaction or the thermal dissociation of $NO_3$, or is confined to the photochemistry. However, the conical intersection at extended $NO_3$ geometries between the ground- and excited-state potential energy surfaces, which has been proposed to lead to the observed multistate dynamics, should be equally accessible by bimolecular and thermal reactions. Whether excited-state roaming is widespread, or constitutes a unique feature of the $NO_3$ system, remains to be seen.

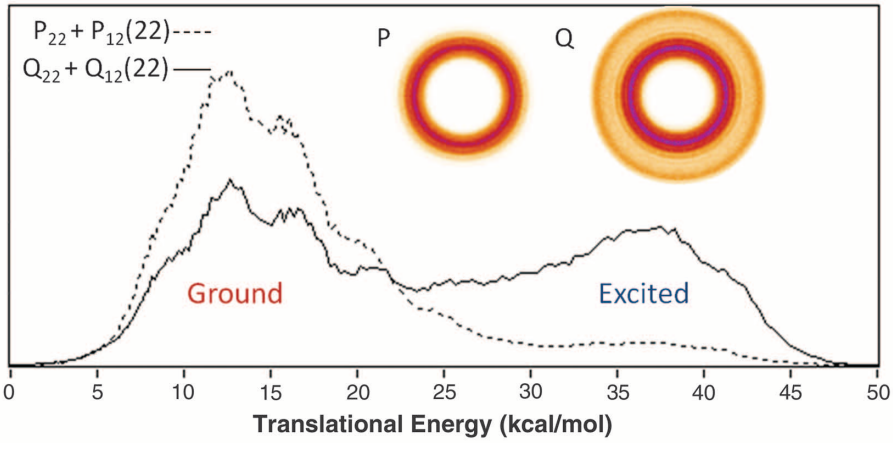


**Fig. 3.** Total translational energy distributions obtained from ion images of the NO photoproduct ($^2\Pi_{3/2}$, $v = 0$, $N = 22$) probing the $P_{22} + P_{12}(22)$ (dashed) and $Q_{22} + Q_{12}(22)$ (solid) transitions, demonstrating the relative Λ doublet propensities of the two reaction channels (*23*).


**References and Notes**

1. J. M. Bowman, B. C. Shepler, *Annu. Rev. Phys. Chem.* **62**, 531 (2011).
2. N. Herath, A. G. Suits, *J. Phys. Chem. Lett.* **2**, 642 (2011).
3. J. Mikosch *et al.*, *Science* **319**, 183 (2008).
4. R. D. van Zee, M. F. Foltz, C. B. Moore, *J. Chem. Phys.* **99**, 1664 (1993).
5. D. Townsend *et al.*, *Science* **306**, 1158 (2004).
6. P. L. Houston, S. H. Kable, *Proc. Natl. Acad. Sci. U.S.A.* **103**, 16079 (2006).
7. B. R. Heazlewood *et al.*, *Proc. Natl. Acad. Sci. U.S.A.* **105**, 12719 (2008).
8. L. B. Harding, S. J. Klippenstein, *J. Phys. Chem. Lett.* **1**, 3016 (2010).
9. M. P. Grubb, M. L. Warter, A. G. Suits, S. W. North, *J. Phys. Chem. Lett.* **1**, 2455 (2010).
10. H. Y. Xiao, S. Maeda, K. Morokuma, *J. Phys. Chem. Lett.* **2**, 934 (2011).
11. S. W. North, *Nat. Chem.* **3**, 504 (2011).
12. M. P. Grubb, M. L. Warter, K. M. Johnson, S. W. North, *J. Phys. Chem. A* **115**, 3218 (2011).
13. I. W. M. Smith, R. P. Tuckett, C. J. Whitham, *Chem. Phys. Lett.* **200**, 615 (1992).
14. K. M. Christoffel, J. M. Bowman, *J. Phys. Chem. A* **113**, 4138 (2009).
15. A. G. Suits, *Acc. Chem. Res.* **41**, 873 (2008).
16. K. Mikhaylichenko, C. Riehn, L. Valachovic, A. Sanov, C. Wittig, *J. Chem. Phys.* **105**, 6807 (1996).
17. P. Andresen, G. S. Ondrey, B. Titze, *Phys. Rev. Lett.* **50**, 486 (1983).
18. Materials and methods are detailed in the supporting online material at *Science* Online.
19. Recent vector correlation measurements of the NO fragment show strong perpendicular correlations between the NO velocity and its rotation, consistent with in-plane dissociation.

20. Although the predicted in-plane abstraction of the oxygen atom may at first seem at odds with the geometrically unconstrained abstraction observed in previous roaming systems, we contend that forces acting as the products separate are governed by the exit channel of the corresponding bimolecular abstraction reaction. Any constraints on the bimolecular reaction should therefore also apply to roaming and will vary for different molecular systems.
21. F. Lahmani, C. Lardeux, D. Solgadi, *Chem. Phys. Lett.* **129**, 24 (1986).
22. M. J. Bronikowski, R. N. Zare, *Chem. Phys. Lett.* **166**, 5 (1990).
23. The two translational distributions have been area normalized for comparison purposes. Absolute propensities are difficult to obtain from our experiment, but maximum propensity calculations necessitate that these normalizations are coincidently approximately correct.

**Acknowledgments:** We acknowledge G. Hall and P. Dagdigian for helpful discussions on Λ doublets and their dynamical implications. Support for this project was provided by the Robert A. Welch Foundation (A-1405), by a grant from the Japan Science and Technology Agency with Core Research for Evolutional Science and Technology (CREST) in the Area of High Performance Computing for Multiscale and Multiphysics Phenomena at Kyoto University, and by a grant from the U.S. Air Force Office of Scientific Research (grant FA9550-10-1-0304) at Emory University.

**Supporting Online Material**
www.sciencemag.org/cgi/content/full/335/6072/1075/DC1
Materials and Methods
Fig. S1
Reference (*24*)

21 November 2011; accepted 6 January 2012
10.1126/science.1216911

# High-Latitude Dust Over the North Atlantic: Inputs from Icelandic Proglacial Dust Storms

**Joseph M. Prospero,[1] Joanna E. Bullard,[2]* Richard Hodgkins[2]**

**Mineral aerosols play an important role in the atmosphere-ocean climate system. Research has focused almost exclusively on sources in low-latitude arid regions, but here we show that there are substantial sources in cold, higher latitudes. A 6-year record of measurements made on Heimaey, an island south of Iceland, reveals frequent dust events with concentrations exceeding 20 micrograms per cubic meter. Much of this potentially iron-rich dust is transported southward and deposited in the North Atlantic. Emissions are highest in spring and spatially and temporally associated with active glacial outwash plains; large dust events appear to be associated with glacial outburst floods. In response to global warming, ice retreat on Iceland and in other glacierized areas is likely to increase dust emissions from these regions.**

Mineral dust aerosols affect climate directly by scattering and absorbing solar and terrestrial radiation and indirectly by affecting cloud properties and, in turn, the hydrological cycle (*1*, *2*). Moreover, dust is an important source of iron (Fe), which in soluble form is an essential micronutrient in marine biota; consequently, dust inputs to the oceans can affect primary productivity and, in turn, the global carbon cycle (*3*, *4*). This is not only a contemporary phenomenon; evidence from terrestrial (loess) and ice core records shows increased dust activity associated with glacial periods that has been linked to the carbon cycle and long-term climate change (*5*–*7*). Accordingly, there is considerable interest in the global distribution of dust sources (*8*), factors affecting dust emissions, and the properties of emitted particles; there are major efforts to model these processes on a global scale (*4*–*9*).

Thus far, research efforts have focused almost exclusively on tropical and mid-latitude arid regions that clearly are major global dust sources (*8*). However, substantial dust events also occur in higher latitudes, particularly in proglacial and paraglacial regions (*10*–*12*). Dust emissions in high latitudes are not confined to arid regions and can occur in humid areas such as Alaska, New Zealand, Patagonia, and Iceland (*10*–*14*). In ice-proximal areas, this is due to limited vegetation cover, high meltwater sediment supply, and strong katabatic or density-driven downglacier winds (*11*, *12*, *15*). Near ice sheets winds driven by steep regional or continental pressure gradients are important. To date, most measurements of high-latitude dust emissions have been confined to individual dust events (storms) or single seasons. Here we report a 6-year data set of aerosol emissions from Iceland.

Daily dust aerosol measurements were made at Stórhöfði, located on the southern tip of the island Heimaey, 17 km off the south coast of Iceland (Fig. 1). A detailed description of the site and sampling protocols are available as supporting online material (SOM) on *Science* Online. Data for February 1997 to December 2002 are shown in Fig. 2, along with data from October to November 2004, when intense dust activity was reported on Iceland.

Dust is present year-round at concentrations of a few micrograms per cubic meter, but occasionally, concentrations increase sharply (Fig. 2). Concentrations exceeded 20 μg $m^{-3}$ in 53 filter samples exposed over a total of 150 days and exceeded 50 μg $m^{-3}$ in 26 filters exposed over 71 days. The highest concentration in our entire record occurred on 19–20 October 2004 and was 1400 μg $m^{-3}$; the daily average concentration over the period 15 to 22 October was 555 μg $m^{-3}$. The original objective was to study pollution from the low latitudes; consequently, the sampler is controlled by wind direction to a 180° sector centered on due south. It therefore does not collect aerosols transported directly to the site by northerly winds; dust is sampled only after winds subsequently shift into sector, a frequent occurrence under typical weather conditions in the region. Thus, the concentrations reported here are minimum estimates of the actual values in plumes crossing the coast.

Dust activity is greatest in spring and early summer (Fig. 2C and table S1); concentrations >20 μg $m^{-3}$ occurred most frequently in April (19 filter samples over 43 days) and May (14 samples over 41 days). The dust events in Fig. 2 are not associated with peaks in nonseasalt $SO_4^=$ or $NO_3^-$, which might have suggested that the dust was transported from Europe in pollution events or dust events from Africa (*16*), but they are instead linked to dust storms on Iceland. Forward air parcel trajectories from Stórhöfði calculated by use of the Hybrid Single-Particle Lagrangian Integrated Trajectory (HYSPLIT) Model (*17*) indicate that much of this dust is transported over the Atlantic Ocean. Trajectories for days when dust concentration exceeded 50 μg $m^{-3}$ reveal that after 120 hours, 14 (39%) of the air masses associated with dust events remained over the North Atlantic, and consequently, the dust was most likely deposited in the marine system. Of the remainder, 13 (36%) made landfall within 120 hours on the west coast of Ireland or the UK; the remaining trajectories reached Norway, France, southern Greenland, or elsewhere in southern Iceland.

To set Icelandic contributions of dust to the Atlantic in context, mineral dust concentrations measured at seven other North Atlantic locations are shown in Fig. 3. The highest concentrations are measured at Cape Verde and Izaña (Tenerife, Canary Islands), reflecting their proximity to Saharan dust sources (*8*, *18*). Dust is transported westward across the North Atlantic and subsequently recorded at samplers in Cayenne, Barbados, Miami, and Bermuda. Dust concentrations recorded at Mace Head, Ireland are generally low (maximum monthly mean, 1.4 μg $m^{-3}$ from 1989 to 1994) with the highest concentrations in the winter and spring (*18*), some of which may be attributable to Icelandic sources. Dust concentrations measured at Stórhöfði are comparable with those reported from Miami and Bermuda; however,

[1]Division of Marine and Atmospheric Chemistry and Cooperative Institute for Marine and Atmospheric Studies, Rosenstiel School of Marine and Atmospheric Science, University of Miami, 4600 Rickenbacker Causeway, Miami, FL 33149, USA. [2]Polar and Alpine Research Centre, Department of Geography, Loughborough University, Leicestershire LE11 3TU, UK.

*To whom correspondence should be addressed. E-mail: j.e.bullard@lboro.ac.uk